Quantum dot quantum cascade photodetector using a laser structure

Fengjiao Wang (王风娇)[1], Ning Zhuo (卓 宁)[1], Shuman Liu (刘舒曼)[1,2,*], Fei Ren (任 飞)[1], Shenqiang Zhai (翟慎强)[1], Junqi Liu (刘俊岐)[1,2], Jinchuan Zhang (张锦川)[1], Fengqi Liu (刘峰奇)[1,2], and Zhanguo Wang (王占国)[1]

[1]*Key Laboratory of Semiconductor Materials Science, Institute of Semiconductors, Chinese Academy of Sciences, Beijing Key Laboratory of Low Dimensional Semiconductor Materials and Devices, Beijing 100083, China*

[2]*College of Materials Science and Opto-Electronic Technology, University of Chinese Academy of Sciences, Beijing 100049, China*

**Corresponding author: liusm@semi.ac.cn*

Received April 18, 2017; accepted July 14, 2017; posted online August 9, 2017

We report on a quantum dot quantum cascade detector (QD-QCD), whose structure is derived from a QD cascade laser. In this structure, more ordered InAs QD layers formed in the Stranski–Krastanow growth mode on a thin GaAs buffer layer are incorporated into the active region. This QD-QCD can operate up to room temperature with a peak detection wavelength of 5.8 μm. A responsivity of 3.1 mA/W at 160 K and a detectivity of 3.6×10^8 Jones at 77 K are obtained. The initial performance of the detector is promising, and, by further optimizing the growth of InAs QDs, integrated QD-quantum cascade laser/QCD applications are expected.

OCIS codes: 230.5590, 040.3060, 040.5570, 230.5160.
doi: 10.3788/COL201715.102301.

Quantum cascade lasers (QCLs) as one kind of intersubband (ISB) laser source have been studied extensively over the past two decades, and their excellent performances have had a profound effect on spectral applications from the infrared to terahertz[1–8]. Meanwhile quantum cascade detectors (QCDs) as one kind of ISB detector have also drawn much attention due to their design freedom and, most importantly, their negligible dark current[9–19]. Actually, the concept of QCD was brought out in the year 2002 when Hofstetter *et al.* used QCL structures as photodetectors[20]. Later, the structures of QCDs were optimized on GaAs-based[21] and InP-based[22] systems, respectively.

Similar to the birth of QCD, interband cascade detectors (ICDs) were also reported in 2005 by using the interband cascade laser structures[23]. It turns out that by using the core of a laser as a detector, the initial performance is promising. The investigations on lasers as photodetectors give us a hint that a miniature integrated sensor may be achieved on-chip by using QCL/QCD with the same structure. In 2014, instead of adopting discrete optical components, Schwarz *et al.* presented a monolithically integrated sensor based on mid-infrared absorption spectroscopy, where a bi-functional QCL/QCD structure on one chip was used[24]. The on-chip sensing of chemicals is in the liquid phase, and the system covers a wide range of concentrations (0–60%) with capabilities to reach parts per million (ppm) accuracy, showing that a monolithically integrated laser/detector is a promising compact system.

Recently, InAs quantum dots (QDs) were incorporated into the InGaAs/InAlAs quantum well (QW) in the active regions of QCLs[25] and QCDs[26]. Theoretically, three-dimensionally confined electrons in QDs have longer lifetimes due to the phonon bottleneck effect[27]. Thus, with a longer lifetime of electrons on the upper lasing state, a lower threshold current density and a higher characteristic temperature of a QD-QCL are expected. While for a QD-QCD, the longer lifetime of electrons on the final state in the absorption region means a higher escape probability for the electrons travelling to the extraction region and, therefore, a higher responsivity. Experimentally, a QD-QCD with InAlAs/InAs(QDs)/GaAs/InGaAs hybrid regions as the absorption regions showed temperature independent infrared response to normal incidence at 4.3 μm and an escape probability of more than 50% for the excited electrons to the extraction region, which were ascribed to the phonon bottleneck effect of the QDs[28]. Similar results were also obtained in the long wavelength infrared quantum dash (QDash) QCDs[29]. On the other hand, a QD-QCL with InAlAs/InAs(QDs)/GaAs/InGaAs hybrid regions in the active region exhibited a high characteristic temperature of threshold current density of about 400 K, but a relatively large threshold current density of 5.36 kA/cm^2[25].

InAs nanostructures grown on InP-based InGaAs/InAlAs material system tend to be QDashes rather than QDs due to the lower strain induced by the underlying buffer material. In order to restrain the appearance of unavoidable InAs QDashes due to the rather small lattice mismatch between InAs and InAlAs, a two-step strain-compensation strategy in the Stranski–Krastanov mode was adopted in our previous QD-QCL and QD-QCD structures[25,26]. The InAs QDs were grown on the tensile strained InAlAs layer and capped by a GaAs buffer layer to increase the lattice mismatch between InAs and the embedded material system. This technique indeed produced QDs instead of QDashes, and this design of the

whole InAlAs/InAs(QDs)/GaAs/InGaAs hybrid region was strain compensated, which is of vital importance in the molecular beam epitaxy (MBE) growth. However, the previous devices did not exhibit desirable high performances mainly due to the nonuniformity in QD sizes. Since InAs QDs can be readily grown on the GaAs/AlGaAs material system because of their larger lattice mismatch, more patterned and uniform QDs can be obtained. Thereby, a new hybrid QD/QW design of InAlAs/GaAs/InAs(QDs)/InGaAs was adopted in the core structures of QD-QCLs aiming at improving the uniformity of the QDs and, therefore, improving the overall performances of the device. In our new design, a thin GaAs buffer layer was inserted on top of $In_{0.44}Al_{0.56}As$ right before the deposition of InAs to take advantage of the large lattice mismatch between InAs and GaAs for the formation of self-assembled InAs QDs. In this way, a performance-improved QD-QCL with threshold current density as low as 1.89 kA/cm^2 and operating temperatures as high as 110°C in pulsed operational mode were demonstrated[30]. To explore the possibility of QD-QCL/QCD integration, we investigated in this Letter the performances of the new QD-QCL structure as a photodetector.

The structures were grown by the MBE technique on semi-insulating InP (100) substrates. One period of the active region consists of a QW/QD hybrid absorption region, which is composed of InAlAs/GaAs/InAs(QD)/InGaAs layers and an extraction region, which is formed by an $In_{0.6}Ga_{0.4}As/In_{0.44}Al_{0.56}As$ chirped superlattice. Twenty-five periods were inserted between a 400 nm thick n-doped (1×10^{18} cm^{-3}) $In_{0.53}Ga_{0.47}As$ bottom contact layer and a 200 nm thick n-doped (1×10^{18} cm^{-3}) $In_{0.53}Ga_{0.47}As$ top contact layer. As shown in Fig. 1, the thickness of the epitaxial layers in the growth sequence starting from the absorption region is as follows (in angstroms, from right to left): **10**/*6.2*/9.3(InAs)/37.4/**8**/18/**40**/29/**34**/31/**24**/33/**17**/36/**14**/5/7.5(InAs)/30.4/**11**/*5.6*/8.5(InAs)/34, with InAlAs in bold, InGaAs in regular, GaAs in italic, and the doping region underlined (Si, 1×10^{18} cm^{-3}). The InAs QDs were obtained by self-assembly on the GaAs layer in the Stranski–Krastanow growth mode, and the growth rate was about 0.4 mono-layers/s. After the QD layer was deposited, 30 s of ripening time was given under arsenic pressure protection. Two simplified samples with the QD/QW hybrid region between two thick InAlAs barriers instead of the cascade region, where sample P1 with InAlAs/InAs(QD)/GaAs/InGaAs layers as the hybrid region and sample P2 with InAlAs/GaAs/InAs(QD)/InGaAs layers as the hybrid region, were grown for photoluminescence (PL) measurements.

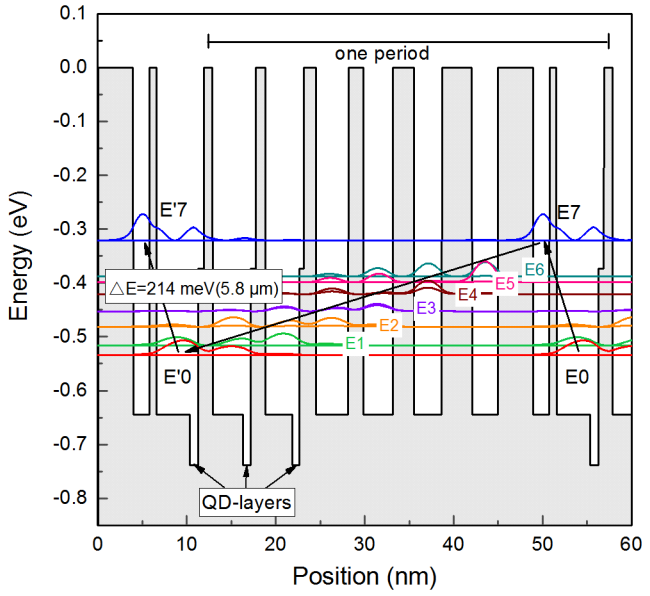

Fig. 1. (Color online) Energy band diagram of one period of the QD-QCD.

Detectors with a mesa of 200 μm × 200 μm were fabricated by standard photolithography, wet chemical etching, metal deposition (Ti/Au), and lift-off process. Then, they were mounted to a copper heat sink and attached to the cold finger of a temperature-controlled liquid nitrogen cryostat to perform the spectral and electrical measurements.

To evaluate the performances of the QD-QCD, we studied the photoresponse, polarization characteristic, and dark current–voltage characteristics of this device. Spectral measurements were performed with a Nicolet 8700 Fourier transform infrared spectrometer (FTIR) in the normal incident configuration for the sake of convenience, and the responsivity was calibrated by a blackbody at 1000 K. The morphology of the QDs was characterized by atomic force microscopy (AFM) AR MFP-3D origin microscope. A low temperature PL measurement was done through a FTIR at 10 K with a 532 nm laser as the excitation source. Dark currents were measured using a Keithley 2635B source meter through the direct current measurement mode, and the samples were all optically and thermally shielded.

A conduction band scheme of one period of the active region at zero bias is shown in Fig. 1. The design calculation was based on the one-dimensional Schrödinger equation under envelope-function approximation for simplicity. The ground state energy E0 in the QW/QD hybrid region was determined experimentally from the PL measurement, as shown in Fig. 2. The energy dependence of the effective mass and the strain of the InAs layer with respect to the InP substrate have been included in the calculation. As mentioned above, the active region consisted of a hybrid absorption region and an extraction region. The dominant transition excited by infrared radiation was between levels E0 and E7 in two adjacent wells with an energy difference of 214 meV, leading to a detection wavelength of 5.8 μm. Here, in this QD-QCD structure, the transition of the electrons excited by the absorbed light is in a diagonal way, similar to the transition in Ref. [31]. Different from the classical vertical transition, the diagonal transition generally yield higher extraction efficiency and higher resistance than vertical transition, leading to an improved overall performance.

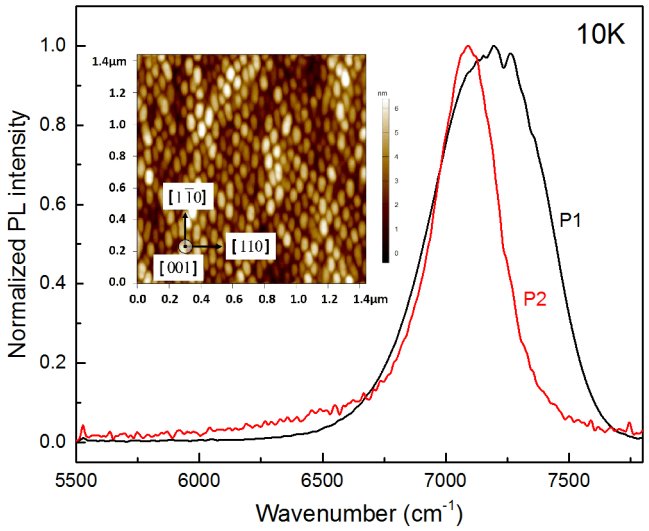

Fig. 2. (Color online) PL spectrum of the simplified QD-QCD structure. The inset shows the AFM image of the QD layer.

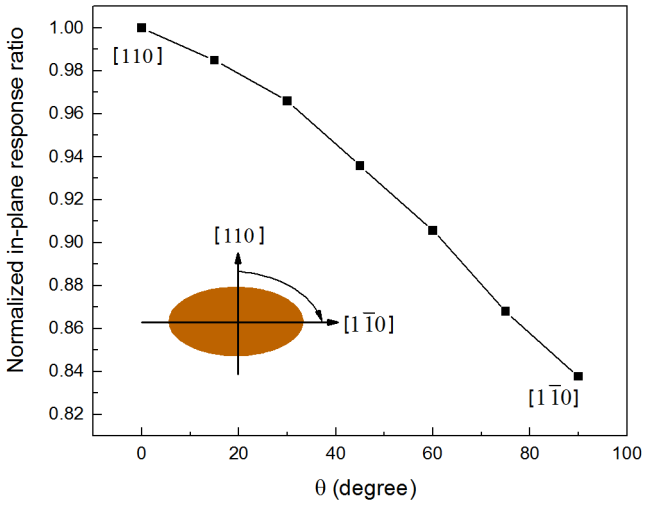

Fig. 3. Normalized in-plane response ratio for QD-QCD from the [110] axis to the [1$\bar{1}$0] axis.

In this case, the energy space between level E7 and E6 is 67 meV∼ two times of a longitudinal optical phonon energy, which assures the extraction efficiency from level E7 to E6. When the electrons reach level E6, they undergo a ministep process from level E5 to level E'0 in the next period, which is similar to the design of a very-long-wavelength infrared detector in Ref. [17]. All of the processes mentioned above generate an electronic displacement under illumination through a cascade of quantum levels without the need of an applied bias.

Figure 2 shows the PL spectra of two simplified samples at 10 K. The peak of PL spectrum of sample P2 lies in 7088 cm^{-1}, ascribing to the interband radiative transition in the hybrid QD/QW region. By comparing with the band gap of the $In_{0.6}Ga_{0.4}As$, we experimentally obtained the energy of the ground level E0 as 0.11 eV from the bottom of conduction band. The inset in Fig. 2 shows the AFM image of the uncapped QD layer in the hybrid absorption region on top of the device structure. As seen, the surface is almost fully covered with InAs dots in an ordered arrangement, aligning in the [1$\bar{1}$0] direction. The size of the dots deduced from the AFM measurement is ∼97 nm along the [1$\bar{1}$0] axis, ∼48 nm along the [110] axis, and ∼3.2 nm in height along the [001] axis, therefore the dot density in the order of 1×10^{10} cm^{-2} was obtained. Compared with the previously designed QDs, the modified QDs are in a more uniform pattern, which can be deduced from the PL spectra. The PL spectrum of the previous designed sample P1 presents a full width at half-maximum (FWHM) of 538 cm^{-1}, and the modified sample P2 presents a decreased value of 301 cm^{-1}, which corresponds to the reduced size distribution.

The in-plane polarized response as a function of the light polarization angle θ was also measured at 77 K, as depicted in Fig. 3. Normalized by the response in the [110] direction, a monotonous decreasing of the intensity of photoresponse versus polarization angle was observed. The normal incident response decreased by about 17% when the polarization was changed from the [110] axis (short) to the [1$\bar{1}$0] axis (long). As a comparison, a controlled QW-QCD was also measured for the in-plane polarized response, and a decrease of 11% was observed, which reveals the anisotropy of the quantum confinements in-plane for the hybrid structure.

Figure 4 shows the photocurrent spectra measured at 77 and 300 K at zero bias voltage with the main peak lying in 1755 cm^{-1}, corresponding to 5.8 μm. A weak side peak lying in 1220 cm^{-1} originated from transitions between level E0 and level E5/E6. The other two weaker peaks lying in 2560 and 3080 cm^{-1} originated from the transitions between ground level E0 to the higher excited levels in the absorption hybrid region, which were negligible and not shown in Fig. 1. The peak responsivity versus temperature from 77 to 300 K in every 20 K is shown in the inset of

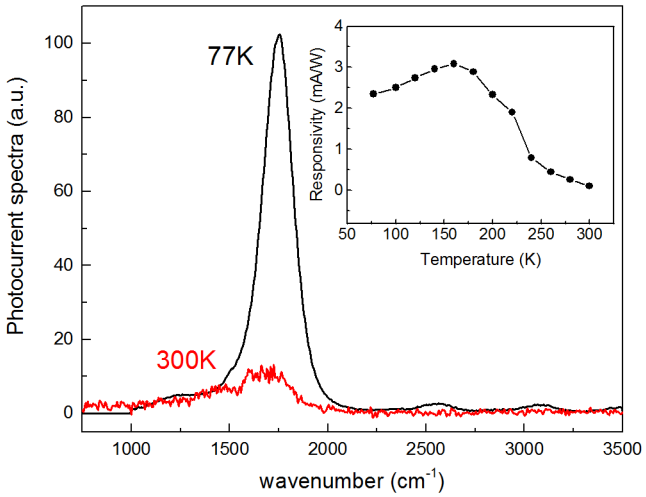

Fig. 4. (Color online) Photocurrent spectra of the QD-QCD at 77 and 300 K. The inset shows the peak responsivity of the device from 77 to 300 K in every 20 K.

Fig. 4. A responsivity of 3.1 mA/W was achieved at 160 K, and it still held a value of 0.11 mA/W at 300 K. It deserves to be mentioned that in the work of Hofstetter *et al.* the photocurrent spectra at zero applied bias showed three main peaks from their standard laser structures, and, for the mid-wave device, a very weak responsivity of 120 μA/W at 2200 cm^{-1} was achieved at 325 K. Different from the results achieved in Ref. [20], our device presents one dominating response peak similar to the classical QCDs, and peak responsivity in the magnitude of mA/W was observed, indicating the potential of a bi-functional lasing/detecting structure with the incorporation of QDs.

Figure 5 shows the dark current versus voltage from 77 to 300 K in every 20 K. The current density around zero bias is about 10^{-4} A/cm^2 at 77 K, which is a desirable value. The low dark current originates mainly from its photovoltaic working scheme and partially from the 3D confinement of QDs. The product of resistance at the zero bias by area of the mesa (R_0A) at different temperatures was obtained from the dark *I*-*V* curves and were plotted in Fig. 6 as a function of inverse of temperature. This value is essential because the high temperature performance of the QD-QCD is mainly limited by Johnson noise. According to the equation $D_J^* = R_p\sqrt{R_0A/(4k_BT)}$, where R_p is peak responsivity, R_0A is the product of resistance at zero bias by the area of the mesa, k_B is the Boltzmann constant, and T is temperature; Johnson noise limited detectivity can be obtained. Figure 6 also shows the detectivity versus temperature from 77 to 300 K in every 20 K. A detectivity of 3.63×10^8 Jones was achieved at 77 K, and this value decreased to 3.47×10^5 at 300 K. The overall performance of the device has been obviously improved compared to the devices reported in Ref. [25]. The highest response temperature of 160 K and an almost negligible photoresponse were obtained in the previous sample with nonuniformity InAs QDs formed on InAlAs. Thus, similar to the improved performances of the new laser structure, the high working temperature and increased responsivity of this new structure as detector are ascribed to the uniformity of InAs QDs. Meanwhile, it is noticed that the size of the InAs QDs is a little large as far as the quantum confinement effect is concerned, and the growth of homogenous InAs QDs with reduced sizes is under investigation for further improved lasing and detecting performances.

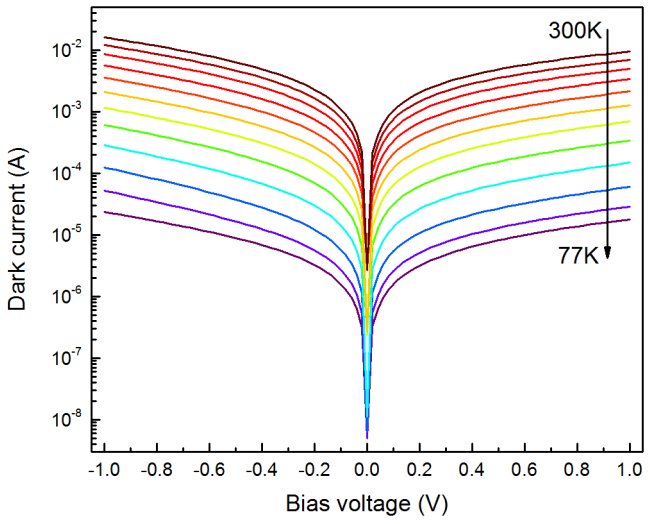

Fig. 5. (Color online) *I*-*V* curves measured under dark condition at temperatures from 77 to 300 K in every 20 K.

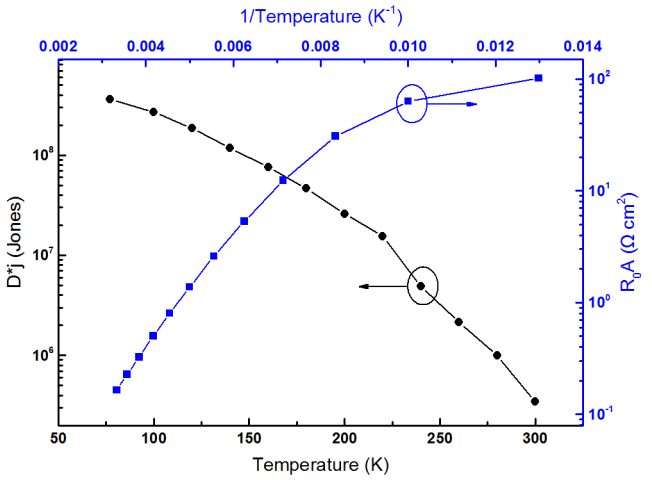

Fig. 6. (Color online) Dependence of R_0A and D_J^* on temperature from 77 to 300 K.

In conclusion, to explore the possibility of a monolithically integrated quantum cascade system, i.e., a QCL/QCD system, based on a QW/QD hybrid design, a QD-QCD with the structure originating from a QD cascade laser is demonstrated. By mainly modifying the growth of the InAs QDs on the GaAs layer instead of on the InAlAs layer in the Stranski–Krastanow growth mode, more patterned QD layers with uniform QDs and desirable performances are achieved. The QD-QCD with a response wavelength of 5.8 μm can operate up to room temperature in photovoltaic mode, which is desirable for a compact sensing system.

This work was supported by the National Basic Research Program of China (No. 2013CB632804/02) and the National Natural Science Foundation of China (Nos. 61376501, 61404131, and 11274301). The authors would like to thank Ping Liang and Ying Hu for their help in device processing.

References

1. J. Faist, F. Capasso, D. L. Sivco, C. Sirtori, A. L. Hutchinson, and A. Y. Cho, Science **264**, 553 (1994).
2. S. Kumar, Chin. Opt. Lett. **9**, 110003 (2011).
3. Q.Y. Lu, Y. Bai, N. Bandyopadhyay, S. Slivken, and M. Razeghi, Appl. Phys. Lett. **97**, 231119 (2010).
4. J. Chen, J. Liu, T. Wang, F. Liu, and Z. Wang, Chin. Opt. Lett. **11**, S20401 (2013).
5. H. Wu, L. Wang, F. Liu, H. Peng, J. Zhang, C. Tong, Y. Ning, and L. Wang, Chin. Opt. Lett. **11**, 091401 (2013).
6. M. A. Belkin, F. Capasso, A. Belyanin, D. L. Sivco, A. Y. Cho, D. C. Oakley, C. J. Vineis, and G. W. Turner, Nat. Photon. **1**, 288 (2007).

7. C. W. Liu, S. Q. Zhai, J. C. Zhang, Y. H. Zhou, Z. W. Jia, F. Q. Liu, and Z. G. Wang, J. Semicond. **36**, 094009 (2015).
8. A. A. Kosterev and F. K. Tittel, IEEE J. Quantum Electron. **38**, 582 (2002).
9. A. Harrer, R. Szedlak, B. Schwarz, H. Moser, T. Zederbauer, D. MacFarland, H. Detz, A. M. Andrews, W. Schrenk, B. Lendl, and G. Strasser, Sci. Rep. **6**, 21795 (2016).
10. A. Harrer, B. Schwarz, S. Schuler, P. Reininger, A. Wirthmuller, H. Detz, D. Macfarland, T. Zederbauer, A. M. Andrews, M. Rothermund, H. Oppermann, W. Schrenk, and G. Strasser, Opt. Express **24**, 17041 (2016).
11. A. Gomez, M. Carras, A. Nedelcu, E. Costard, X. Marcadet, and V. Berger, Proc. SPIE **6900**, 69000J (2008).
12. F. R. Giorgetta, E. Baumann, M. Graf, Q. K. Yang, C. Manz, K. Köhler, H. E. Beere, D. A. Ritchie, E. Linfield, A. G. Davies, Y. Fedoryshyn, H. Jäckel, M. Fischer, J. Faist, and D. Hofstetter, IEEE J. Quantum Electron. **45**, 1039 (2009).
13. A. Buffaz, M. Carras, L. Doyennette, A. Nedelcu, P. Bois, and V. Berger, Proc. SPIE **7660**, 76603Q (2010).
14. S. Q. Zhai, J. Q. Liu, X. J. Wang, S. Tan, F. Q. Liu, and Z. G. Wang, Infrared Phys. Technol. **63**, 17 (2014).
15. S. Sakr, E. Giraud, A. Dussaigne, M. Tchernycheva, N. Grandjean, and F. H. Julien, Appl. Phys. Lett. **100**, 181103 (2012).
16. N. Kong, J. Q. Liu, L. Li, F. Q. Liu, L. J. Wang, Z. G. Wang, and W. Lu, Chin. Phys. Lett. **27**, 128503 (2010).
17. S. Q. Zhai, J. Q. Liu, X. J. Wang, N. Zhuo, F. Q. Liu, Z. G. Wang, X. H. Liu, and W. Lu, Appl. Phys. Lett. **102**, 191120 (2013).
18. M. Graf, G. Scalari, D. Hofstetter, J. Faist, H. Beere, E. Linfield, D. Ritchie, and G. Davies, Appl. Phys. Lett. **84**, 475 (2004).
19. X. J. Wang, J. Q. Liu, S. Q. Zhai, F. Q. Liu, and Z. G. Wang, J. Semicond. **35**, 104009 (2014).
20. D. Hofstetter, M. Beck, and J. Faist, Appl. Phys. Lett. **81**, 2683 (2002).
21. L. Gendron, C. Koeniguer, V. Berger, and X. Marcadet, Appl. Phys. Lett. **86**, 121116 (2005).
22. M. Graf, N. Hoyler, M. Giovannini, J. Faist, and D. Hofstetter, Appl. Phys. Lett. **88**, 241118 (2006).
23. J. V. Li, R. Q. Yang, C. Hill, and S. L. Chuang, Appl. Phys. Lett. **86**, 101102 (2005).
24. B. Schwarz, P. Reininger, D. Ristanic, H. Detz, A. M. Andrews, W. Schrenk, and G. Strasser, Nat. Commum. **5**, 4085 (2014).
25. N. Zhuo, F. Q. Liu, J. C. Zhang, L. J. Wang, J. Q. Liu, S. Q. Zhai, and Z. G. Wang, Nanoscale Res. Lett. **9**, 144 (2014).
26. X. J. Wang, S. Q. Zhai, N. Zhuo, J. Q. Liu, F. Q. Liu, S. M. Liu, and Z. G. Wang, Appl. Phys. Lett. **104**, 171108 (2014).
27. J. Urayama, T. B. Norris, J. Singh, and P. Bhattacharya, Phys. Rev. Lett. **86**, 4930 (2001).
28. F. J. Wang, N. Zhuo, S. M. Liu, F. Ren, Z. D. Ning, X. L. Ye, J. Q. Liu, S. Q. Zhai, F. Q. Liu, and Z. G. Wang, Appl. Phys. Lett. **108**, 251103 (2016).
29. F. J. Wang, F. Ren, S. M. Liu, N. Zhuo, S. Q. Zhai, J. Q. Liu, F. Q. Liu, and Z. G. Wang, Nanoscale Res. Lett. **11**, 392 (2016).
30. N. Zhuo, J. C. Zhang, F. J. Wang, Y. H. Liu, S. Q. Zhai, Y. Zhao, D. B. Wang, Z. W. Jia, Y. H. Zhou, L. J. Wang, J. Q. Liu, S. M. Liu, F. Q. Liu, Z. G. Wang, J. B. Khurgin, and G. Sun, Opt. Express **25**, 13807 (2017).
31. P. Reininger, B. Schwarz, H. Detz, D. MacFarland, T. Zederbauer, A. M. Andrews, W. Schrenk, O. Baumgartner, H. Kosina, and G. Strasser, Appl. Phys. Lett. **105**, 091108 (2014).